doi:10.1016/j.jmb.2011.09.021 J. Mol. Biol. (2011) 413, 804–814

Contents lists available at www.sciencedirect.com

Journal of Molecular Biology

journal homepage: http://ees.elsevier.com.jmb

Cyt1Aa Toxin: Crystal Structure Reveals Implications for Its Membrane-Perforating Function

Shmuel Cohen[1,2]†, Shira Albeck[3]†, Eitan Ben-Dov[1,4], Rivka Cahan[2], Michael Firer[2], Arieh Zaritsky[1] and Orly Dym[3]*

[1]*Department of Life Sciences, Ben-Gurion University of the Negev, Be'er-Sheva 84105, Israel*
[2]*Department of Chemical Engineering and Biotechnology, Ariel University Center of Samaria, Ariel 40700, Israel*
[3]*Israel Structural Proteomics Center, Department of Structural Biology, Weizmann Institute of Science, Rehovot 76100, Israel*
[4]*Achva Academic College, MP Shikmim 78900, Israel*

Received 16 June 2011; received in revised form 9 September 2011; accepted 13 September 2011
Available online 19 September 2011

Edited by I. Wilson

Keywords:
Bacillus thuringiensis israelensis;
Cyt2Aa;
Cyt2Ba;
Cyt1Ca;
VVA2

During sporulation, *Bacillus thuringiensis* subsp. *israelensis* produces a mosquito larvicidal protein complex containing several crystalline and cytolytic (Cyt) toxins. Here, the activated monomeric form of Cyt1Aa, the most toxic Cyt family member, was isolated and crystallized, and its structure was determined for the first time at 2.2 Å resolution.

Cyt1Aa adopts a typical cytolysin fold containing a β-sheet held by two surrounding α-helical layers. The absence of a β-strand (between residues V26 and I37) in the dimeric structure of Cyt2Aa led us to deduce that this is the only essential segment for dimer formation and that activation of the toxin occurs by proteolytic processing of its N-terminus. Based on the Cyt1Aa structure, we suggest that the toxicity of Cyt1Aa and other nonrelated proteins, all sharing a cytolysin fold, is correlated with their ability to undergo conformational changes that are necessary prior to their membrane insertion and perforation. This fold allows the α-helical layers to swing away, exposing the β-sheet to insert into the membrane. The identification of a putative lipid binding pocket between the β-sheet and the helical layer of Cyt1Aa supports this mechanism. Sequence-based structural analysis of Cyt1Aa revealed that the lack of activity of Cyt1Ca may be related to the latter's inability to undergo this conformational change due to its lack of flexibility. The pattern of the hemolytic activity of Cyt1Aa presented here (resembling that of pore-forming agents), while differing from that imposed by ionic and nonionic detergents, further supports the pore-forming model by which conformational changes occur prior to membrane insertion and perforation.

Introduction

The toxicity of the Gram-positive bacterium *Bacillus thuringiensis* (widely used as a biological alternative to chemical pesticides) to insects is due to δ-endotoxic crystals composed of a series of proteins that react with the cells lining the larval midgut of susceptible insects.[1] Insecticidal proteins are produced during sporulation and classified into two

*Corresponding author. E-mail address: orly.dym@weizmann.ac.il.

† S.C. and S.A. contributed equally to this work.

Abbreviations used: Cyt, cytolytic; Cry, crystalline; PDB, Protein Data Bank; VVA2, volvatoxin A2; RBC, red blood cell.

families of membrane-perforating toxins, crystalline (Cry) and cytolytic (Cyt), that are packed into a paracrystalline structure. Following ingestion by an insect of its host range, the Cry and Cyt toxic crystals are solubilized, and their protoxins are cleaved by alkaline-active digestive enzymes at the high pH prevailing in the larval midgut.[2,3] The activated Cry toxins bind to specific protein receptors located on the host cell surface, oligomerize, and insert into the membrane, forming lytic pores that cause cell swelling and lysis.[4–7] In contrast, Cyt toxins do not bind specific receptors but act nonspecifically by direct interaction with membrane lipids.[8–11] However, there is an assumption that the toxicity of Cyt1Aa may be related to the specific unsaturated fatty acid composition of lipids in the midgut epithelial cells of Diptera insects. For example, incubation of Cyt1Aa with lipids extracted from *Aedes albopictus* larvae neutralized its activity, while incubation with *Bacillus megaterium* membranes did not neutralize toxin activity.[11]

Both types of toxins, Cry and Cyt, act by destroying cell membranes, but the latter is less specific, causing *in vitro* lysis of a broad range of insect and mammalian cells.[12–14] The two families share no common sequence or structural resemblance. They have distinct secondary structures: the α-helical regions of Cry toxins form the transmembrane pore, whereas Cyt toxins are presumed to be inserted into the membrane by a β-barrel composed of β-sheet hairpins from each monomer.[7,15,16] Other toxins of the α-helical class include colicins, exotoxin A, and diphtheria, whereas aerolysin, α-hemolysin (α-toxin), anthrax-protective antigen, and cholesterol-dependent toxins (e.g., perfringolysin O) belong to the β-barrel group.[16]

Cyt proteins have a single α/β domain composed of two outer layers of α-helix hairpins wrapped around a β-sheet.[9] So far, three families of Cyt proteins, Cyt1 and Cyt2, and Cyt3 (data for Cyt3 unpublished), have been identified‡. Cyt1 and Cyt2 are produced *in vivo* as protoxins and undergo activation by the removal of small portions of their N-termini and C-termini.[9] Most of the known Cyt proteins are encoded by *B. thuringiensis* subspecies that are specific against the larvae of Diptera insects. Subspecies *israelensis*, which is widely exploited commercially to control mosquitoes, includes Cry (−4Aa, −4Ba, −10Aa, and −11Aa) and Cyt (−1Aa and −2Ba) proteins that act jointly to kill mosquito larvae.[17,18] Lack of resistance to *B. thuringiensis* subsp. *israelensis* in nature may stem from the synergistic interactions between the different Cry toxins and Cyt1Aa.[19,20] Point mutations in Cry11Aa and Cyt1Aa that affect the binding and the synergy between them and inhibit the formation of the prepore oligomer and membrane perforation have been described. It has been suggested that Cyt1Aa synergizes Cry11Aa in the formation of Cry11Aa prepore and pore oligomeric structures.[21]

The mechanism by which Cyt1Aa damages cell membrane is still a subject of debate. The conventional model for Cyt proteins suggests that the monomer undergoes conformational changes such that, upon membrane contact, the two outer α-helical layers swing away from the β-sheet that is inserted into the membrane. Oligomerization of Cyt monomers on the cell membrane forms β-barrel pores[15,16] that induce colloid-osmotic lysis (i.e., equilibration of ions), followed by a net influx of water, cell swelling, and eventual lysis.[9,22,23] It has been proposed that the pores formed by the toxin are assembled by three major β-strands (β6–β8) present in the C-terminal domain of Cyt1Aa.[10] This model has been confirmed by the findings that a recombinant N-terminal domain of Cyt1Aa (containing the helical layers) lost its hemolytic and insecticidal activities and induced its self-aggregation in solution, whereas a recombinant C-terminal domain composed mainly of the β-sheet (β6–β8) was found to be responsible for the interaction of the toxin with the lipid membrane.[24] This further supports the finding that the N-terminal domain was removed when the membrane-bound Cyt1Aa was treated with protease.[3] An alternative mode of action, known as the detergent-like mechanism, presumes that the Cyt proteins do not perforate the membrane but rather adsorb as aggregates onto the surface, thereby causing defects in membrane packing that enable leakage of intracellular molecules.[11,25]

The gene *cyt1Aa* was the first member of the *cyt* family to be isolated and studied,[26] but attempts to obtain *in vitro* Cyt1Aa diffractive crystals failed due to the tendency of the naive protein to aggregate and precipitate.[27] In this study, we adapted a partial endogenous cleavage technique to obtain a soluble toxic form of monomeric Cyt1Aa cleaved mostly at its N-terminus. This enabled crystallization and determination of its structure, homologous to those of the corresponding regions of Cyt2Aa[9] and Cyt2Ba.[28] Extensive sequence-based structural analysis of Cyt1Aa and comparison to that of the nontoxic Cyt1Ca[17,29,30] highlight possible explanations for the lack of toxicity of the latter. The analysis supports the mechanism by which Cyt1 family members undergo conformational changes prior to their membrane insertion and perforation. This is reinforced by the pattern of the hemolytic activity of Cyt1Aa, which resembles that of the pore-forming agents α-toxin[31,32] and saponin[33] but differs from that imposed by the ionic and nonionic detergents sodium dodecyl sulfate (SDS) and Triton X-100, respectively.

‡ www.lifesci.sussex.ac.uk/home/Neil_Crickmore/Bt/index.html

Results and Discussion

The overall structure of monomeric Cyt1Aa

The currently known subfamily members of Cyt1 (1Aa, 1Ab, 1Ba, and 1Ca) and Cyt2 (2Aa, 2Ba, 2Bb, 2Bc, and 2Ca) share a high level of sequence identity (Fig. 1). The Cyt1Aa dimer undergoes endogenous proteolysis, removing small portions of its termini and resulting in a monomeric activated toxin (Fig. S1) that crystallizes readily. This fragment between N38 and L249 corresponds to the N-terminal proteolytically cleaved segments of Cyt2Aa and Cyt2Ba.[8,9,35,36] Since M1-I37 at the N-terminus and only S243-L249 at its C-terminus are missing, it is reasonable to assume that mainly the N-terminus is truncated. The crystal structure of Cyt1Aa, resolved at 2.2 Å resolution (Table 1), has a typical cytolysin fold and is composed of a single domain of α/β architecture consisting of a central β-sheet surrounded by two α-helical layers (Fig. 2a). The sheet consists of six main β-strands arranged in space as follows: β1↑, β5↓ (together forming a single noncontinuous strand), β6↑, β7↓, β8↑, and β4↓. The sheet is flanked by two α-helical layers: α1 and α2 on one side, and α3–α6 on the other. In addition, Cyt1Aa contains an insertion of a β-hairpin (β2–β3) between α1 and α2. This hairpin is common to all members of the Cyt1 family, while it is absent in the Cyt2 family (Figs. 1 and 2a). The four longest β-strands (β4 and β6–β8) of the central β-sheet have a modified Greek key topology composed of β6–β8 connected by a longer link to β4, which is adjacent to the first strand β6. The structure is characterized by two internal salt-bridge contacts between residues R78-E196 and K163-D72, which hold the β-hairpin to the β-sheet (Fig. 2a). The model consists of two monomers in the asymmetric unit for which electron densities exist for residues N38-I238 in monomer A and for residues N38-T242 in monomer B (with 31 water molecules). The N38-T242 fragment is calculated to be ~22.4 kDa, in accordance with the molecular mass of the truncated fragment observed on SDS-PAGE (Fig. S1).

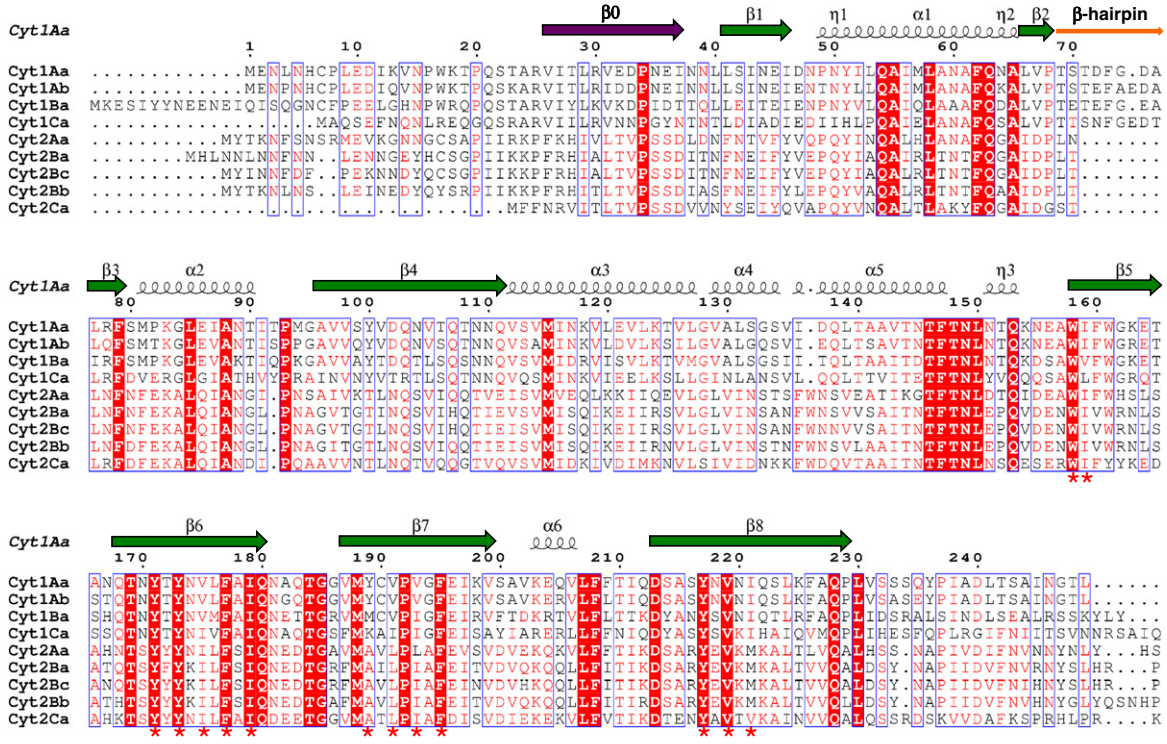

Fig. 1. Sequence alignment of Cyt1 and Cyt2 family members. Cyt1Aa secondary structure elements are labeled above the corresponding sequence; α-helices and η-helices are depicted as spirals, and β-strands are depicted as arrows. Numbers refer to the Cyt1Aa sequence. The residues conserved in all four proteins are shown in red blocks. β0 of the dimeric structure of Cyt2Aa (PDB code: 1CBY), corresponding to residues V26-I37 in Cyt1Aa, is designated in purple. The extra residues participating in the β-hairpin (unique to the Cyt1 family) are marked with an orange arrow. The conserved hydrophobic residues forming the putative lipid binding pocket are marked by red asterisks. Note that only the N-terminal segment of Cyt1Ca that is homologous to Cyt1Aa is presented in this alignment. The figure was created using ESPript.[34]

Table 1. Data collection and structure refinement statistics

Data collection	
Resolution range (Å)	50.0–2.2 (2.24–2.20)
Space group	$P2_12_12_1$
Unit cell dimensions	
a (Å)	33.89
b (Å)	65.82
c (Å)	176.53
Number of molecules in the asymmetric unit	2
Number of reflections measured	370,403
Number of unique reflections[a]	20,996 (954)
Number of reflections used for refinement	19,384
R_{sym}[a]	0.107 (0.376)
Completeness (%)	99.0 (92.6)
Redundancy	6.8 (6.2)
$\langle I\rangle/\langle\sigma(I)\rangle$	17.05 (3.3)
Refinement statistics	
Resolution limits (Å)	50.0–2.2
R_{free}[b] (%)	26.07
R_{work}[b] (%)	19.53
Number of water molecules	31
Mean *B*-factor for protein atoms (Å^2)	28.8
Mean *B*-factor for waters (Å^2)	30.4
RMSD	
Bond lengths (Å)	0.017
Bond angles (°)	1.54
Torsion angles (°)	12.98
Ramachandran plot	
Most favored regions (%)	91.4
Additionally allowed regions (%)	8.4
Generously allowed regions (%)	0.3
Disallowed regions (%)	0.0

Values in parentheses are for the highest-resolution shells.

[a] $R_{sym} = \sum |\langle I_{hkl}\rangle - I_{hkl}| / I_{hkl}$, where $\langle I_{hkl}\rangle$ is the average intensity over symmetry-related reflections and I_{hkl} is the observed intensity.

[b] $R = \sum||F_o| - |F_c||/\sum|F_o|$, where F_o denotes the observed structure factor amplitude and F_c is the structure factor calculated from the model.

Comparison of Cyt1Aa with structurally related proteins supports the pore-forming model

A striking similarity between the structure of the cleaved Cyt1Aa monomer (residues N38-T242), the endogenously cleaved Cyt2Ba monomer [Protein Data Bank (PDB) code 2RCI],[28] and the corresponding region of Cyt2Aa (PDB code: 1CBY) was observed.[9] Full-length Cyt2Aa forms a dimer by extensive interactions involving residues from β0 and β1 and residues S233-D240 from the C-terminus (Cyt1Aa numbering; Fig. 1).[9] The two β-strands of monomer A (β0 and β1) of Cyt2Aa are intertwined with the corresponding strands in monomer B, forming a β-sheet.[9] The structure of the Cyt1Aa monomer contains β1 (L41-I46) and the C-terminal segment (S233-D240); nevertheless, the protein does not dimerize. It therefore appears that β0, which is absent in the Cyt1Aa structure, is the only essential segment for dimer formation and that activation of the toxin occurs by proteolytic processing of the protein's N-terminus.

The structures of the monomers of Cyt1Aa, Cyt2Ba, and Cyt2Aa resemble that of the toxic volvatoxin A2 (VVA2; PDB code: 1VCY) despite their low (under 20%) sequence identity.[39] A structural overlay of the Cyt1Aa and VVA2 structures demonstrates a perfect alignment of their corresponding β-sheets, while deviations are observed between the two α-helical layers (Fig. 2c). The largest structural deviation occurs in the β-hairpin (β2–β3) inserted between α1 and α2, which is common to both Cyt1Aa and VVA2 (Figs. 2a and 2c, pink arrows). The model of cytolysis proposed for VVA2 involves two steps.[40] The VVA2 protein is thought to initially bind the cell membrane and then forms oligomers by exposing its amphipathic α-helix. This results in permeabilization of the cell membrane by insertion of β-barrels formed by β-strands 5, 6, and 7 (VVA2 numbering). The corresponding α3 of Cyt1Aa also exerts an amphipathic character, supporting a similar perforating mechanism.

Cyt1Aa, like other Cyt family members, also has a fold similar to that of the virulence factor Evf (PDB code: 2W3Y)[39] despite its very low (12%) sequence identity.[38] While Evf is covalently bound to palmitate, none of the Cyt family members contains a palmitoylated Cys residue. In the Evf structure, the lipid is found in a hydrophobic pocket embedded between the β-sheet composed of β3 and β5–β7 and helices α4 and α5 (Evf numbering).[41] It has been suggested that the lack of toxicity of Evf may be due to the presence of the covalently bound palmitate.[36] The structural homology between Cyt1Aa and Evf enabled the identification of a putative fatty acid binding site in Cyt1Aa between the sheet formed by β4, β6–β8, and helices α3–α5, similar to that identified in Cyt2Ba.[38] Conserved hydrophobic residues in the β-sheets of the Cyt family members have been suggested to point their side chains towards the putative binding site rather than towards the opposite side of the sheet.[38] Indeed, the Cyt1Aa structure displays the conserved hydrophobic residues pointing towards the putative lipid binding pocket (Figs. 1 and 2b). We suggest that, in Evf, the covalently bound lipid "locks" the helical layer to the β-sheet and prevents the conformational changes necessary for membrane insertion, explaining its observed nontoxicity.[42] On the other hand, the absence of the lipid in Cyt1Aa enables its flexibility and allows the conformational changes in the two surrounding α-helical layers of Cyt1Aa necessary for exposing the hydrophobic β-sheet. The putative lipid binding site also provides an explanation for the binding specificity for unsaturated membrane phospholipids, which has been observed for Cyt1Aa.[10]

The high structural similarity despite the low sequence identity observed between the Cyt family members VVA2 and Evf supports the importance of their cytolysin fold for activity. We suggest that their

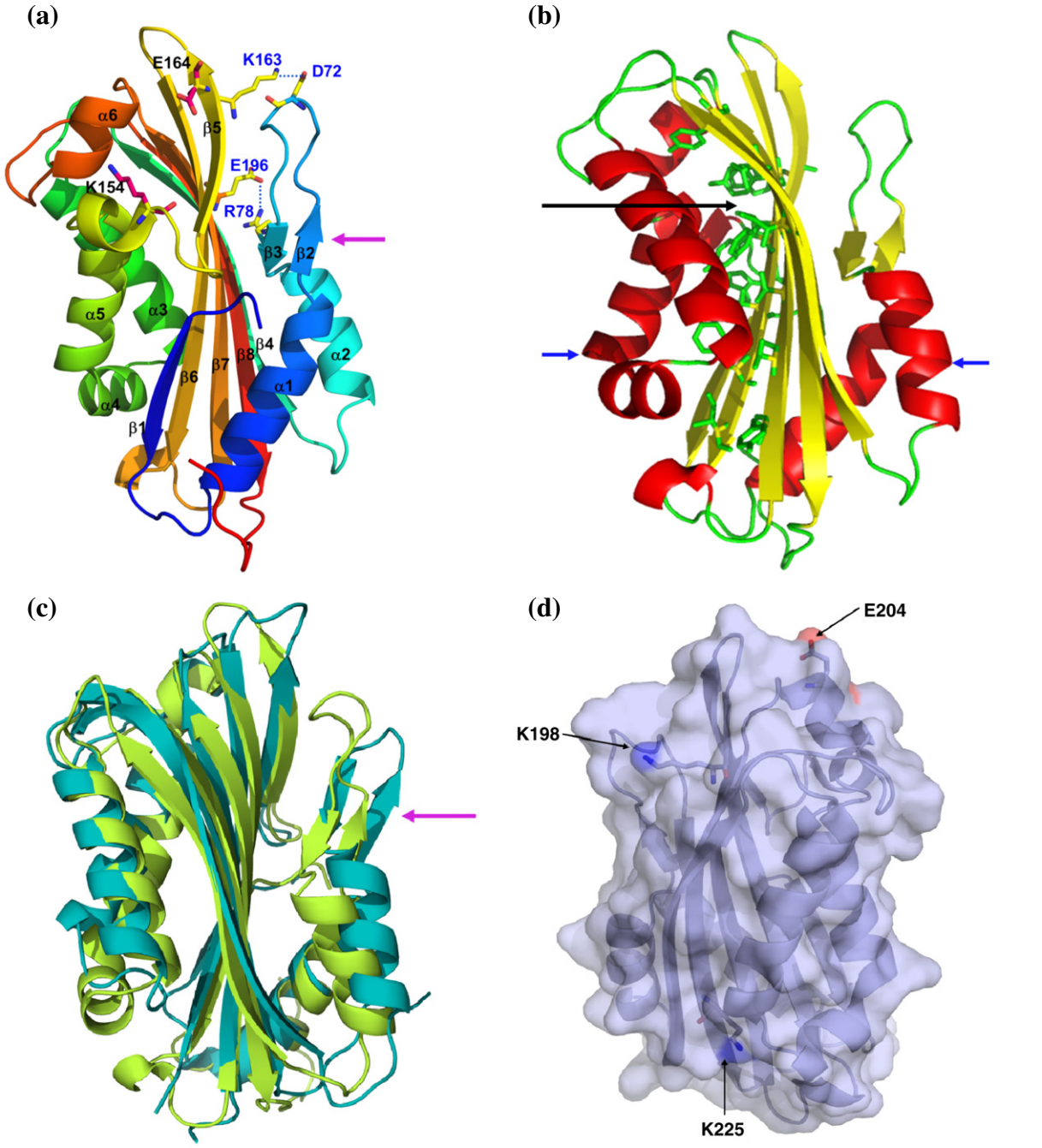

Fig. 2. Ribbon representation of the monomeric (N38-I242) Cyt1Aa crystal structure. (a) Secondary structure elements (labeled according to Fig. 1) colored in rainbow starting from blue to red (created with PyMOL[37]). The pink arrow designates the β-hairpin that is unique to the Cyt1 family members and to VVA2 (PDB code: 1VCY). Two internal salt bridges between residues R78-E196 and K163-D72 are designated by blue broken lines. Charged residues K154 and E164, which have been identified as important for Cyt1Aa toxicity[29] and are not conserved in Cyt1Ca, are designated by sticks and labeled in red (D240 is not shown, as there is no observed electron density for it). (b) The α/β architecture of the Cyt1Aa monomer, characterized by a central β-sheet (yellow) surrounded by two outer α-helical layers (red). A putative lipid binding site (black arrow) was identified by homology to the structure of Evf (PDB code: 2W3Y[38]). The pocket is lined by conserved hydrophobic residues all pointing towards it (green sticks). The α-helical layers (blue arrows) were proposed[9] to lift upward and away from the sheet, allowing its penetration into the membrane. (c) A structural overlay of Cyt1Aa (green) and VVA2 (cyan; PDB code: 1VCY) showing a perfect alignment of their corresponding β-sheets, while deviations are observed between their α-helical layers. The largest structural deviation occurs in their β-hairpin (pink arrow), which is common to both proteins. (d) Surface representation of Cyt1Aa (transparent blue) showing secondary structure. The acidic exposed residues that interact with and synergize the activity of Cry11Aa (K198, E204, and K225) are shown with sticks and designated by arrows.

toxicity is correlated with their ability to undergo conformational changes prior to membrane insertion and perforation. While electrostatic forces may play an important role in the initial association with the membrane,[43] the contact of a fatty acid chain of a membrane with the putative lipid binding site would provide a plausible explanation for the second phase of interaction, since hydrophobic interactions would obviously predominate at the membrane binding site.

Relative toxicities of Cyt1Aa and Cyt1Ca

Cyt1Ca is encoded on the megaplasmid pBtoxis of *B. thuringiensis* subsp. *israelensis* and is neither larvicidal nor hemolytic. It is twice the size of Cyt toxins and is predicted to display the structure of a two-domain fusion protein: an N-terminus that resembles Cyt toxins and a C-terminus that is similar to the receptor binding domain of ricin-B lectin.[17] The C-truncated Cyt1Ca domain (homologous to Cyt1Aa) remains nontoxic,[44] indicating that the C-terminus is not responsible for its lack of toxicity.

In an attempt to understand why Cyt1Ca is nontoxic, we performed a comparative sequence analysis of all known Cyt1 family members revealing that Cyt1Ca is the most divergent. The residues that are conserved in Cyt1Aa, Cyt1Ab, and Cyt1Ba, but differ in Cyt1Ca, are labeled with asterisks in Fig. S2a and are mapped onto the structure of Cyt1Aa (Fig. S2b). Interestingly, many of the nonconserved residues in Cyt1Ca are located on the α-helical layers and on strands β1, β4, and β5, which have been proposed to undergo conformational changes upon membrane binding. The contribution of these residues to the lack of toxicity of Cyt1Ca was supported by the finding that mutating three of these nonconserved residues (Q154, Q164, and G240) in Cyt1Ca to the corresponding charged and exposed residues in Cyt1Aa (K154, E164, and D240, respectively) restored partial antibacterial—although not larvicidal—activities, indicating their importance (Fig. 2a).[29] Interestingly, many of the charged residues that have been identified as important for Cyt1Aa toxicity (E45, R78, K124, K154, K163, E164, K203, E204, D213, K225, and D240; Fig. S2c)[20] are conserved in Cyt1Ca (D45, R78, K124, R163, R203, and D213), suggesting that the lack of toxicity of Cyt1Ca may result from other factors as well.

Taken together with the position of the nonconserved residues in Cyt1Ca on the α-helical layers and on β1, β4, and β5, we suggest that the lack of toxicity may also be related to the lack of flexibility. This is supported by the finding that substitution of Q225 in Cyt1Ca to the corresponding conserved K225 in Cyt1Aa does not restore activity.[26] This residue is located on β8, which is part of the sheet thought to insert into the membrane.[19,20] We postulate that the location of the nonconserved residues in Cyt1Ca may render this protein unable to undergo the conformational changes associated with membrane insertion, thereby explaining its nontoxicity.

Mapping Cyt1Aa essential residues for binding Cry11Aa and Cry4Ba onto its structure

Cyt1Aa synergizes the activities of particular Cry toxins in *B. thuringiensis* subsp. *israelensis*.[45] Specifically, binding of Cry11Aa to brush border membrane vesicles of *Aedes aegypti* larvae is enhanced by membrane-bound Cyt1Aa. Two binding epitopes of Cyt1Aa—$_{196}$EIKVSAVKE$_{204}$ (locating on β7 and α6) and $_{220}$NIQSLKFAQ$_{228}$ (locating on β8) (Fig. 1)—were found to be involved in the binding interaction with Cry11Aa.[21] Both regions are mostly embedded, with only $_{200}$SAVKE$_{204}$ exposed. The role of these epitopes was confirmed by heterologous competition assays using synthetic peptides corresponding to these regions and by site-directed mutagenesis.[21] In particular, three single residues (K198, E204, and K225) within these two segments were shown to be involved in the interaction between these two proteins, in turn explaining the synergism between them.[21] Recently, it has been shown that mutation of these Cyt1Aa residues affects Cyt1Aa's binding and synergism with Cry4Ba as well.[46] Interestingly, these three residues are charged in most of the Cyt1 family members, whereas they are polar (T198, Q204, and T225, respectively, in Cyt2Ba; Fig. 1) in the Cyt2 family and in Cyt1Ca, which presumably do not bind Cry11Aa. Thus, it seems reasonable that the synergism and binding of Cyt1Aa to Cry11Aa or Cry4Ba depend on specific interactions between these toxins, which involve these residues. We suggest that the reduced charge on Cyt2 protein members and on Cyt1Ca may be sufficient to abrogate binding to Cry11Aa. It was suggested that mutating these residues in other Cyt proteins to the corresponding Cyt1Aa charged residues might introduce binding sites and induce synergism with Cry toxins. This strategy could be used as a tool to overcome Cry resistance in the midgut membrane of resistant insects.[47]

A sequential mechanism by which Cyt1Aa initially undergoes conformational changes to insert its β-sheet into the membrane following binding of Cry11Aa *via* the two Cyt1Aa binding epitopes, resulting in insertion of Cry11Aa into the mosquito membranes, has been proposed.[22] Mapping the three charged residues on the Cyt1Aa structure (Fig. 2d) revealed that while all three residues are exposed to the surface of the protein, they all reside on regions of the toxin that presumably are inserted into the membrane (K198 and E204 are located on β7 and α6, and K225 is part of β8). We therefore cannot rule out an alternative mechanism by which Cyt1Aa

binds Cry11Aa using these exposed charged residues prior to its membrane insertion. Thus, the action of Cyt1Aa alone or as a receptor for Cry11Aa may involve different mechanisms.

The hemolytic activity of Cyt1Aa supports the membrane pore-forming mechanism

Under various stress conditions, normal red blood cells (RBCs) change their shape from normal discocytes to echinocytes, spherocytes, and, finally, empty ghost cells. The *in vitro* crenation process (echinocytosis) occurs upon metabolic changes in normal discocytes caused by various agents such as alkaline pH,[48] ATP depletion,[49] metabolic starvation, phospholipid incorporation,[50] nonionic amphiphilic compounds,[51] Ca^{2+},[48,52] and ethanol.[53] On the other hand, discocyte-to-stomatocyte (cup-shaped cells) transformation is thought to be caused by cationic amphiphiles. It was shown that alkyl-trimethylammonium salts and SDS, which induce echinocytic shapes in rat RBCs, further inverted into discocytes and stomatocytes as the incubation proceeded, as the concentration increased, or upon cooling to room temperature.[54] It was also shown that RBCs exposed to dodecyl-zwittergent or SDS attained a stomatocytic shape when washed in a buffer containing bovine serum albumin.[55]

According to the model of perforation by Cyt1Aa, the integrity of the cell membrane remains intact, but the flow of cations through the pores disturbs the osmotic balance of the cell. Thus, leakage of ATP from cells and elevation of intracellular Ca^{2+} caused by Cyt1Aa would be expected to result in echinocytosis, as happens with other perforating proteins such as mellitin, gramicidin S, α-toxin from *Staphylococcus aureus*, and adenylate cyclase toxin (CyaA) from *Bordetella pertussis*.[56] This type of morphological change is expected to differ from that caused by detergents. On the other hand, if the Cyt proteins act through a detergent-like mechanism, the hemolytic pattern would resemble that incurred by anionic detergents such as SDS, since the estimated net charge of activated Cyt1Aa (22.4 kDa) is negative (−5.1) at neutral pH.

To distinguish between these alternatives, we compared the hemolytic activity of the isolated monomeric form of Cyt1Aa and the morphology of the exposed RBCs to those affected by the following agents: (i) α-toxin, thought to create β-barrel pores in the cell membrane;[31,32] (ii) saponin, a plant-derived surfactant that removes membrane-anchored cholesterol and produces permanent 4-nm-diameter to 5-nm-diameter holes, leading to echinocytosis and cells lysis;[33] (iii) SDS, an ionic detergent; and (iv) nonionic Triton X-100. The HC_{50} of Cyt1Aa was in the nanomolar range, similar to that observed for α-toxin, whereas both ionic and nonionic detergents exhibited hemolysis in the micromolar range (Fig. 3). The extent of hemolysis increased gradually with the concentrations of both α-toxin and Cyt1Aa, whereas with Triton X-100 and SDS, it increased sharply from 2–3% to 92–98% at a concentration range of 100–200 and 50–100 μM, respectively. Both detergents lysed almost 100% of the RBCs at a concentration of 200 μM, which is near the critical micellar concentration of Triton X-100. The hemolytic pattern of saponin was unique: it exhibited gradual concentration dependence as Cyt1Aa and α-toxin, while its active concentration range (5–100 μM) was similar to that observed with SDS and Triton X-100.

The morphological changes in RBCs exposed to serial dilutions of toxins/detergents were analyzed (Fig. S3). Cells exposed to each of the toxins exhibited shapes corresponding to normal discocytes, echinocytes, spherocytes, and ghosts (Fig. S3a–f), whereas cells exposed to detergents transformed into stomatocytes, spherocytes, and ghosts, but not to echinocytes (Fig. S3h–m). Saponin produced an intermediate state where echinocytes formed at sublytic concentrations and stomatocytes formed at lytic concentrations (Fig. S3n–p). Thus, the morphological effect of Cyt1Aa resembles that of α-toxin.

The relative changes in cell morphologies were plotted from randomly acquired frames (Fig. S4). The general morphological pattern induced by Cyt1Aa is similar to that of α-toxin and different from that of the detergents. Both Cyt1Aa and α-toxin at concentrations of 20 nM and above caused the number of normal discocytes to decrease and the number of echinocytes to increase up to ~20%. At this concentration, spherocytes (mainly in cells

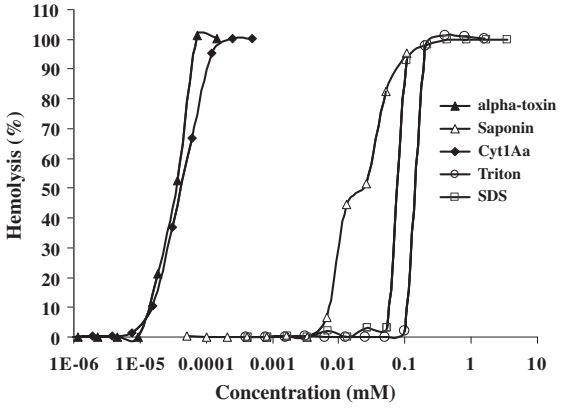

Fig. 3. Hemolysis of RBCs treated with Cyt1Aa compared to SDS, Triton X-100, α-toxin, and saponin. The concentration at which 50% of RBCs lyse (HC_{50}) is 44.3 and 34.9 nM for Cyt1Aa and α-toxin, respectively, and 25.47, 84.5, and 150 μM for saponin, SDS, and Triton X-100, respectively. Results represent the average of three independent experiments.

exposed to α-toxin) appear together with ghosts, empty cells, and lysis (Fig. S4a and b). This hemolytic pattern is totally different from that caused by SDS and Triton X-100 (Fig. S4c and d). Under sublytic concentrations of 20–50 μM (<3% hemolysis), there was a dramatic increase of up to 75% stomatocytes (instead of echinocytes observed with Cyt1Aa and α-toxin). At higher detergent concentrations, there was an increase in the number of spherocytes and ghost cells, but almost no echinocytes were observed. The hemolytic pattern induced by saponin was a mixture of both characteristics (Fig. S4e). Thus, the relative changes in cell morphology induced by Cyt1Aa are similar to those observed in the presence of α-toxin and different from that of detergents, suggesting a pore-forming mechanism.

A comprehensive study of membrane-active toxins could facilitate the design of targeted drugs.[57,58] The crystal structure of Cyt1Aa and its unique segments described here broaden our understanding of the mechanisms underlying its toxicity and hence significantly contribute to the achievement of this goal.

Materials and Methods

Reagents

SDS was purchased from Fluka (cat. no. 05030); 4-(1,1,3,3-tetra-methyl-butyl)phenyl-polyethylene-glycol (Triton X-100) was purchased from Sigma-Aldrich (cat. no. X-100); *Gypsophila* plant saponin was purchased from Sigma (cat. no. S-1252); and *Staphylococcus aureus* α-toxin was purchased from Calbiochem (cat. no. 616392).

Purification of Cyt1Aa

Cyt1Aa was produced using strain IPS(pHT*cy1Aa-p20*) of acrystalliferous *B. thuringiensis israelensis* IPS 78/11 containing pHT-315-*cyt1Aa-p20*, which expresses *cyt1Aa* and *p20*[59] (encoding a helper protein that enhances the expression of insecticidal crystal proteins in wild-type strains during sporulation[60]). Cyt1Aa was produced as easily isolatable crystals after growth in CCY sporulation medium[61] for 4 days, at which time most cells sporulated and autolysed. The culture was centrifuged, and the sediment, including crystals, spores, and debris, was rinsed thrice with double-distilled water. The pure Cyt1Aa crystals were separated on a discontinuous sucrose gradient,[62] rinsed with water, and solubilized in an alkaline buffer containing 50 mM Na_2CO_3 (pH 10.5) without protease inhibitors. The dissolved crystals were allowed to age for 10 days at 4 °C, during which time spontaneous proteolysis occurred. Dimeric nonproteolyzed Cyt1Aa was separated from the monomeric proteolyzed fraction by size-exclusion chromatography (HiLoad 16/60 Superdex75; GH Healthcare) and equilibrated with a 20 mM (pH 7.5) Hepes buffer containing 50 mM NaCl, 5% glycerol, and 5 mM DTT. The eluted peaks were analyzed on 15% SDS-PAGE (Fig. S1). Fractions containing proteolytically cleaved Cyt1Aa were pooled, concentrated by Centricon® centrifugal filter YM-10 (Millipore, Billerica, MA, USA) to 2 mg/ml (determined by OD_{280}), and crystallized.

Crystallization, data collection, and refinement

Single crystals of the proteolytically cleaved Cyt1Aa (residues 38–238) were obtained by the sitting-drop vapor diffusion method, using the mosquito robot. Cyt1Aa crystals were grown from a solution of 20% polyethylene glycol 6000, 0.1 M sodium acetate (pH 5.0), and 0.2 M NH_4Cl. Crystals formed in space group $P2_12_12_1$ with cell constants $a=33.895$ Å, $b=65.822$ Å, and $c=176.534$ Å, and contained two monomers in the asymmetric unit cell with a V_m of 1.8 Å^3/Da. The diffraction data from a single crystal were collected at beamline ID14-4 of the European Synchrotron Radiation Facility, indexed, and integrated using the program HKL2000.[63] Integrated intensities were scaled using the program SCALEPACK.[63] The structure factor amplitudes were calculated using TRUNCATE from the CCP4 program suite. The structure of Cyt1Aa was solved to 2.2 Å resolution by molecular replacement with the program Phaser,[64] using as starting model the known structure of the mosquito larvicidal δ-endotoxin Cyt2Aa from subspecies *kyushuensis* (PDB code: 1CBY). Refinement was carried out using the program CCP4/Refmac5.[65] The model was built to σ_A-weighted, $2F_{obs}-F_{calc}$, and $F_{obs}-F_{calc}$ maps using the program Coot.[66] Water molecules were built into peaks greater than 3σ on $F_{obs}-F_{calc}$ maps. Finally, the Cyt1Aa model was evaluated with the program MolProbity.[67] Data collection and refinement statistics are described in Table 1. The structural figures were created using PyMOL.[37] Sequence alignment was prepared with ESPript.[34]

Hemolysis assay and optical differential interference contrast analysis

Erythrocytes were isolated from whole blood of healthy human donors and subjected to hemolysis assay, as previously described.[59] The sediment of RBC samples exposed to cytotoxins was cooled to room temperature, diluted in the presence of 1% bovine serum albumin (to prevent echinocytosis when pipetted onto glass cover slides), and observed by differential interference contrast using a Zeiss AxioObserver.Z1 inverted microscope (at a magnification of 40× with a 1.6× optovar objective) with a CCD camera (Axiocam HRm; Carl Zeiss). Frames depicting cells were randomly acquired, and 100 cells exposed to each agent at a given concentration were counted. The relative ratio of each cell shape (D, discocytes; E, echinocytes; St, stomatocytes; S, spherocytes; G, ghosts) was recorded and presented as a function of concentration.

PDB accession code

The coordinates of Cyt1Aa have been deposited in the PDB on April 2011 under accession code 3RON.

Supplementary materials related to this article can be found online at doi:10.1016/j.jmb.2011.09.021

Acknowledgements

We thank Prof. Ehud Gazit (Faculty of Life Sciences, Tel-Aviv University) for careful reading of the manuscript and for his constructive comments. We thank Prof. Joel L. Sussman for helpful discussions. The structure of Cyt1Aa was determined at the Israel Structural Proteomics Center. This work was partially supported by grants (2001–042 and 2007–037 to A.Z.) from the United States–Israel Binational Science Foundation (Jerusalem, Israel), the Divadol Foundation, the European Commission Sixth Framework Research, and the Technological Development Program (contract no. 031220).

References

1. Schnepf, E., Crickmore, N., Van Rie, J., Lereclus, D., Baum, J., Feitelson, J. *et al.* (1998). *Bacillus thuringiensis* and its pesticidal crystal proteins. *Microbiol. Mol. Biol. Rev.* **62**, 775–806.
2. Bravo, A., Likitvivatanavong, S., Gill, S. S. & Soberon, M. (2011). *Bacillus thuringiensis*: a story of a successful bioinsecticide. *Insect Biochem. Mol. Biol.* **41**, 423–431.
3. Du, J., Knowles, B. H., Li, J. & Ellar, D. J. (1999). Biochemical characterization of *Bacillus thuringiensis* cytolytic toxins in association with a phospholipid bilayer. *Biochem. J.* **338**, 185–193.
4. Fernandez, L. E., Perez, C., Segovia, L., Rodriguez, M. H., Gill, S. S., Bravo, A. & Soberon, M. (2005). Cry11Aa toxin from *Bacillus thuringiensis* binds its receptor in *Aedes aegypti* mosquito larvae through loop alpha-8 of domain II. *FEBS Lett.* **579**, 3508–3514.
5. Fernandez-Luna, M. T., Lanz-Mendoza, H., Gill, S. S., Bravo, A., Soberon, M. & Miranda-Rios, J. (2010). An alpha-amylase is a novel receptor for *Bacillus thuringiensis* ssp. *israelensis* Cry4Ba and Cry11Aa toxins in the malaria vector mosquito *Anopheles albimanus* (Diptera: *Culicidae*). *Environ. Microbiol.* **12**, 746–757.
6. Likitvivatanavong, S., Chen, J., Evans, A. M., Bravo, A., Soberon, M. & Gill, S. S. (2011). Multiple receptors as targets of cry toxins in mosquitoes. *J. Agric. Food. Chem.* **59**, 2829–2838.
7. Soberon, M., Pardo, L., Munoz-Garay, C., Sanchez, J., Gomez, I., Porta, H. & Bravo, A. (2010). Pore formation by Cry toxins. *Adv. Exp. Med. Biol.* **677**, 127–142.
8. Gill, S. S., Singh, G. J. & Hornung, J. M. (1987). Cell membrane interaction of *Bacillus thuringiensis* subsp. *israelensis* cytolytic toxins. *Infect. Immun.* **55**, 1300–1308.
9. Li, J., Koni, P. A. & Ellar, D. J. (1996). Structure of the mosquitocidal delta-endotoxin CytB from *Bacillus thuringiensis* sp. *kyushuensis* and implications for membrane pore formation. *J. Mol. Biol.* **257**, 129–152.
10. Promdonkoy, B. & Ellar, D. J. (2003). Investigation of the pore-forming mechanism of a cytolytic delta-endotoxin from *Bacillus thuringiensis*. *Biochem. J.* **374**, 255–259.
11. Thomas, W. E. & Ellar, D. J. (1983). Mechanism of action of *Bacillus thuringiensis* var. *israelensis* insecticidal delta-endotoxin. *FEBS Lett.* **154**, 362–368.
12. Chilcott, C. N., Wigley, P. J., Broadwell, A. H., Park, D. J. & Ellar, D. J. (1998). Activities of *Bacillus thuringiensis* insecticidal crystal proteins Cyt1Aa and Cyt2Aa against three species of sheep blowfly. *Appl. Environ. Microbiol.* **64**, 4060–4061.
13. Gill, S. S. & Hornung, J. M. (1987). Cytolytic activity of *Bacillus thuringiensis* proteins to insect and mammalian cell lines. *J. Invertebr. Pathol.* **50**, 16–25.
14. Thomas, W. E. & Ellar, D. J. (1983). *Bacillus thuringiensis* var. *israelensis* crystal delta-endotoxin: effects on insect and mammalian cells *in vitro* and *in vivo*. *J. Cell Sci.* **60**, 181–197.
15. Li, J., Derbyshire, D. J., Promdonkoy, B. & Ellar, D. J. (2001). Structural implications for the transformation of the *Bacillus thuringiensis* delta-endotoxins from water-soluble to membrane-inserted forms. *Biochem. Soc. Trans.* **29**, 571–577.
16. Parker, M. W. & Feil, S. C. (2005). Pore-forming protein toxins: from structure to function. *Prog. Biophys. Mol. Biol.* **88**, 91–142.
17. Berry, C., O'Neil, S., Ben-Dov, E., Jones, A. F., Murphy, L., Quail, M. A. *et al.* (2002). Complete sequence and organization of pBtoxis, the toxin-coding plasmid of *Bacillus thuringiensis* subsp. *israelensis*. *Appl. Environ. Microbiol.* **68**, 5082–5095.
18. Margalith, Y. & Ben-Dov, E. (2000). Biological control by *Bacillus thuringiensis* subsp. *israelensis*. In *Insect Pest Management: Techniques for Environmental Protection* (Rechcigl, J. E. & Rechcigl, N. A., eds), pp. 243–301, Lewis Publishers and CRC Press LLC, Boca Raton, FL.
19. Promdonkoy, B. & Ellar, D. J. (2005). Structure–function relationships of a membrane pore forming toxin revealed by reversion mutagenesis. *Mol. Membr. Biol.* **22**, 327–337.
20. Ward, E. S., Ellar, D. J. & Chilcott, C. N. (1988). Single amino acid changes in the *Bacillus thuringiensis* var. *israelensis* delta-endotoxin affect the toxicity and expression of the protein. *J. Mol. Biol.* **202**, 527–535.
21. Perez, C., Fernandez, L. E., Sun, J., Folch, J. L., Gill, S. S., Soberon, M. & Bravo, A. (2005). *Bacillus thuringiensis* subsp. *israelensis* Cyt1Aa synergizes Cry11Aa toxin by functioning as a membrane-bound receptor. *Proc. Natl Acad. Sci. USA*, **102**, 18303–18308.
22. Bravo, A., Gill, S. S. & Soberon, M. (2007). Mode of action of *Bacillus thuringiensis* Cry and Cyt toxins and their potential for insect control. *Toxicon*, **49**, 423–435.
23. Knowles, B. H., Blatt, M. R., Tester, M., Horsnell, J. M., Carroll, J., Menestrina, G. & Ellar, D. J. (1989). A cytolytic delta-endotoxin from *Bacillus thuringiensis* var. *israelensis* forms cation-selective channels in planar lipid bilayers. *FEBS Lett.* **244**, 259–262.
24. Rodriguez-Almazan, C., Ruiz de Escudero, I., Canton, P. E., Munoz-Garay, C., Perez, C., Gill, S. S. *et al.* (2010). The amino- and carboxyl-terminal fragments of the *Bacillus thuringensis* Cyt1Aa toxin have differential roles in toxin oligomerization and pore formation. *Biochemistry*, **50**, 388–396.
25. Butko, P. (2003). Cytolytic toxin Cyt1A and its mechanism of membrane damage: data and hypotheses. *Appl. Environ. Microbiol.* **69**, 2415–2422.
26. Bourgouin, C., Klier, A. & Rapoport, G. (1986). Characterization of the genes encoding the haemolytic toxin and the mosquitocidal delta-endotoxin of *Bacillus thuringiensis israelensis*. *Mol. Gen. Genet.* **205**, 390–397.

27. McPherson, A., Jurnak, F., Singh, G. J. & Gill, S. S. (1987). Preliminary X-ray diffraction analysis of crystals of *Bacillus thuringiensis* toxin, a cell membrane disrupting protein. *J. Mol. Biol.* **195**, 755–757.
28. Cohen, S., Dym, O., Albeck, S., Ben-Dov, E., Cahan, R., Firer, M. & Zaritsky, A. (2008). High-resolution crystal structure of activated Cyt2Ba monomer from *Bacillus thuringiensis* subsp. *israelensis*. *J. Mol. Biol.* **380**, 820–827.
29. Itsko, M., Manasherob, R. & Zaritsky, A. (2005). Partial restoration of antibacterial activity of the protein encoded by a cryptic open reading frame (cyt1Ca) from *Bacillus thuringiensis* subsp. *israelensis* by site-directed mutagenesis. *J. Bacteriol.* **187**, 6379–6385.
30. Itsko, M. & Zaritsky, A. (2007). Exposing cryptic antibacterial activity in Cyt1Ca from *Bacillus thuringiensis israelensis* by genetic manipulations. *FEBS Lett.* **581**, 1775–1782.
31. Bhakdi, S. & Tranum-Jensen, J. (1991). Alpha-toxin of *Staphylococcus aureus*. *Microbiol. Rev.* **55**, 733–751.
32. Gouaux, E. (1998). Alpha-hemolysin from *Staphylococcus aureus*: an archetype of beta-barrel, channel-forming toxins. *J. Struct. Biol.* **121**, 110–122.
33. Seeman, P., Cheng, D. & Iles, G. H. (1973). Structure of membrane holes in osmotic and saponin hemolysis. *J. Cell Biol.* **56**, 519–527.
34. Gouet, P., Courcelle, E., Stuart, D. I. & Metoz, F. (1999). ESPript: analysis of multiple sequence alignments in PostScript. *Bioinformatics*, **15**, 305–308.
35. Al-yahyaee, S. A. S. & Ellar, D. J. (1995). Maximal toxicity of cloned CytA δ-endotoxin from *Bacillus thuringiensis* subsp. *israelensis* requires proteolytic processing from both the N- and C-termini. *Microbiology*, **141**, 3141–3148.
36. Armstrong, J. L., Rohrmann, G. F. & Beaudreau, G. S. (1985). Delta endotoxin of *Bacillus thuringiensis* subsp. *israelensis*. *J. Bacteriol.* **161**, 39–46.
37. DeLano, W. L. (2002). *The PyMOL Molecular Graphics System.* DeLano Scientific, San Carlos, CA; http://www.pymol.org.
38. Rigden, D. J. (2009). Does distant homology with Evf reveal a lipid binding site in *Bacillus thuringiensis* cytolytic toxins? *FEBS Lett.* **583**, 1555–1560.
39. Lin, S. C., Lo, Y. C., Lin, J. Y. & Liaw, Y. C. (2004). Crystal structures and electron micrographs of fungal volvatoxin A2. *J. Mol. Biol.* **343**, 477–491.
40. Weng, Y. P., Lin, Y. P., Hsu, C. I. & Lin, J. Y. (2004). Functional domains of a pore-forming cardiotoxic protein, volvatoxin A2. *J. Biol. Chem.* **279**, 6805–6814.
41. Quevillon-Cheruel, S., Leulliot, N., Muniz, C. A., Vincent, M., Gallay, J., Argentini, M. *et al.* (2009). Evf, a virulence factor produced by the *Drosophila* pathogen *Erwinia carotovora*, is an S-palmitoylated protein with a new fold that binds to lipid vesicles. *J. Biol. Chem.* **284**, 3552–3562.
42. Acosta Muniz, C., Jaillard, D., Lemaitre, B. & Boccard, F. (2007). *Erwinia carotovora* Evf antagonizes the elimination of bacteria in the gut of *Drosophila* larvae. *Cell. Microbiol.* **9**, 106–119.
43. Manceva, S. D., Pusztai-Carey, M., Russo, P. S. & Butko, P. (2005). A detergent-like mechanism of action of the cytolytic toxin Cyt1A from *Bacillus thuringiensis* var. *israelensis*. *Biochemistry*, **44**, 589–597.
44. Manasherob, R., Itsko, M., Sela-Baranes, N., Ben-Dov, E., Berry, C., Cohen, S. & Zaritsky, A. (2006). Cyt1Ca from *Bacillus thuringiensis* subsp. *israelensis*: production in *Escherichia coli* and comparison of its biological activities with those of other Cyt-like proteins. *Microbiology*, **152**, 2651–2659.
45. Chang, C., Yu, Y. M., Dai, S. M., Law, S. K. & Gill, S. S. (1993). High-level cryIVD and cytA gene expression in *Bacillus thuringiensis* does not require the 20-kilodalton protein, and the coexpressed gene products are synergistic in their toxicity to mosquitoes. *Appl. Environ. Microbiol.* **59**, 815–821.
46. Canton, P. E., Zanicthe Reyes, E. Z., Ruiz de Escudero, I., Bravo, A. & Soberon, M. (2011). Binding of *Bacillus thuringiensis* subsp. *israelensis* Cry4Ba to Cyt1Aa has an important role in synergism. *Peptides*, **32**, 595–600.
47. Bravo, A. & Soberon, M. (2008). How to cope with insect resistance to Bt toxins? *Trends Biotechnol.* **26**, 573–579.
48. Weed, R. I. & Chailley, B. (1972). Calcium–pH interactions in the production of shape change in erythrocytes. *Nouv. Rev. Fr. Hematol.* **12**, 775–788.
49. Nakao, M., Nakao, T. & Yamazoe, S. (1960). Adenosine triphosphate and maintenance of shape of the human red cells. *Nature*, **187**, 945–946.
50. Ferrell, J. E., Jr., Lee, K. J. & Huestis, W. H. (1985). Membrane bilayer balance and erythrocyte shape: a quantitative assessment. *Biochemistry*, **24**, 2849–2857.
51. Park, N. G., Kim, C. H., Chung, J. K., Huh, M. D., Park, J. S. & Kang, S. W. (1998). Morphological changes of biomembranes by amphiphilic basic peptides mastoparan B and 4(3). *J. Microbiol.* **36**, 179–183.
52. White, J. G. (1976). Scanning electron microscopy of erythrocyte deformation: the influence of a calcium ionophore, A23187. *Semin. Hematol.* **13**, 121–132.
53. McLawhon, R. W., Marikovsky, Y., Thomas, N. J. & Weinstein, R. S. (1987). Ethanol-induced alterations in human erythrocyte shape and surface properties: modulatory role of prostaglandin E1. *J. Membr. Biol.* **99**, 73–78.
54. Isomaa, B. & Paatero, G. (1981). Shape and volume changes in rat erythrocytes induced by surface-active alkyltrimethylammonium salts and sodium dodecyl sulphate. *Biochim. Biophys. Acta*, **647**, 211–222.
55. Hagerstrand, H., Bobacka, J., Bobrowska-Hagerstrand, M., Kralj-Iglic, V., Fosnaric, M. & Iglic, A. (2001). Oxyethylene chain–cation complexation: nonionic polyoxyethylene detergents attain a positive charge and demonstrate electrostatic head group interactions. *Cell. Mol. Biol. Lett.* **6**, 161–165.
56. Katsu, T., Kuroko, M., Morikawa, T., Sanchika, K., Fujita, Y., Yamamura, H. & Uda, M. (1989). Mechanism of membrane damage induced by the amphipathic peptides gramicidin S and melittin. *Biochim. Biophys. Acta*, **983**, 135–141.
57. Al-yahyaee, S. A. & Ellar, D. J. (1996). Cell targeting of a pore-forming toxin, CytA delta-endotoxin from *Bacillus thuringiensis* subspecies *israelensis*, by conjugating CytA with anti-Thy 1 monoclonal antibodies and insulin. *Bioconjugate Chem.* **7**, 451–460.
58. Cohen, S., Cahan, R., Ben-Dov, E., Nisnevitch, M., Zaritsky, A. & Firer, M. A. (2007). Specific targeting to murine myeloma cells of Cyt1Aa toxin from *Bacillus*

thuringiensis subspecies *israelensis*. *J. Biol. Chem.* **282**, 28301–28308.
59. Nisnevitch, M., Cohen, S., Ben-Dov, E., Zaritsky, A., Sofer, Y. & Cahan, R. (2006). Cyt2Ba of *Bacillus thuringiensis israelensis*: activation by putative endogenous protease. *Biochem. Biophys. Res. Commun.* **344**, 99–105.
60. Shao, Z. & Yu, Z. (2004). Enhanced expression of insecticidal crystal proteins in wild *Bacillus thuringiensis* strains by a heterogeneous protein P20. *Curr. Microbiol.* **48**, 321–326.
61. Stewart, G. S., Johnstone, K., Hagelberg, E. & Ellar, D. J. (1981). Commitment of bacterial spores to germinate. A measure of the trigger reaction. *Biochem. J.* **198**, 101–106.
62. Debro, L., Fitz-James, P. C. & Aronson, A. (1986). Two different parasporal inclusions are produced by *Bacillus thuringiensis* subsp. *finitimus*. *J. Bacteriol.* **165**, 258–268.
63. Otwinowski, Z. & Minor, W. (1997). Processing of X-ray diffraction data collected in oscillation mode. *Macromolecular Crystallography, Part A*, vol. 276, pp. 307–326Academic Press, Inc., San Diego, CA.
64. McCoy, A. J. (2007). Solving structures of protein complexes by molecular replacement with Phaser. *Acta Crystallogr., Sect. D: Biol. Crystallogr.* **63**, 32–41.
65. Murshudov, G. N., Vagin, A. A. & Dodson, E. J. (1997). Refinement of macromolecular structures by the maximum-likelihood method. *Acta Crystallogr., Sect. D: Biol. Crystallogr.* **53**, 240–255.
66. Emsley, P. & Cowtan, K. (2004). Coot: model-building tools for molecular graphics. *Acta Crystallogr., Sect. D: Biol. Crystallogr.* **60**, 2126–2132.
67. Chen, V. B., Arendall, W. B., III, Headd, J. J., Keedy, D. A., Immormino, R. M., Kapral, G. J. *et al.* (2010). MolProbity: all-atom structure validation for macromolecular crystallography. *Acta Crystallogr., Sect. D: Biol. Crystallogr.* **66**, 12–21.